A Preliminary Evaluation of Icing Scaling on AAM Propellers

Jen-Ching Tsao[1]
Ohio Aerospace Institute, Cleveland, OH, 44142

Zaid Sabri[2], Paul H. von Hardenberg[3]
and Curtis A. Flack[4]
NASA Glenn Research Center, Cleveland, OH, 44135

NASA Glenn Research Center recently developed a general-purpose propeller test stand for conducting fundamental icing physics studies on electrically driven propellers in the Icing Research Tunnel (IRT). Some preliminary icing scaling evaluation tests were conducted on propellers for Advanced Air Mobility (AAM) applications using existing recommended scaling methods that were originally developed for fixed wing aircraft. Three carbon fiber propellers of 24, 28, and 36 inch diameters were used for the test. All three propellers had a NACA 0012 airfoil profile and were geometrically scaled from a radial location of roughly 40% to the tip. During the March 2023 test entry in the IRT, a simplified model size scaling evaluation was performed in a rime ice condition with the three propellers, and a *LWC* condition scaling was evaluated in a glaze ice condition with the 28 inches diameter propeller. In the January 2024 IRT test entry, another *LWC* condition scaling was evaluated on the 36 inches diameter propeller. The ice shape scaling evaluation was performed by extracting 2D ice shapes from 3D laser scans at propeller radial location of 75%. The preliminary ice shape results showed the scaling methods are effective. Further evaluation of the scaling methods is recommended over a wider range of airflow and icing cloud conditions as well as different propeller sizes and operating conditions to assess its applicability for modern propeller and open fan engine icing scaling analysis.

I. Nomenclature

A_c	=	accumulation parameter (Eq. (9))
B	=	Relative heat factor (Eq.(13)),
c	=	airfoil chord
c_p	=	Specific heat of air
$c_{p,ws}$	=	Specific heat of water at the surface temperature
D	=	propeller diameter
d	=	Cylinder diameter or twice the airfoil leading-edge radius
h_c	=	Convective heat-transfer coefficient
h_G	=	Gas-phase mass-transfer coefficient
K	=	Inertia parameter (Eq. (5)),
K_0	=	Modified inertia parameter (Eq. (4)),
J	=	advance ratio
LWC	=	Cloud liquid-water content

[1] Principal Research Scientist, Icing Branch, 21000 Brookpark Rd., MS 11-2, Associate Fellow AIAA
[2] Aerospace Engineer, Icing Branch, 21000 Brookpark Rd., MS 11-2, Member AIAA
[3] Aerospace Engineer, Icing Branch, 21000 Brookpark Rd., MS 11-2, Member AIAA
[4] Aerospace Flight Systems Engineer, Systems Engineering and Architecture Division, 21000 Brookpark Rd., MS-162-4, Member AIAA

MVD = Water droplet median volume diameter
n = freezing fraction
n_0 = freezing fraction at stagnation point (Eq. (10))
n_0^* = theoretical freezing potential at stagnation point
N = propeller rotational speed, rev/s
p = Pressure
p_w = Vapor pressure of water in atmosphere
p_{ww} = Vapor pressure of water at the icing surface
r = radial distance or recovery factor
R = propeller tip radius
Re_δ = Reynolds number of water drop (Eq. (6))
t_f = freezing temperature
t_s = Surface temperature
$t_{0,\infty}$ = freestream total air temperature
T = Absolute air temperature, K
V_{ax} = axial component of air velocity
V_{eff} = effective air velocity
V_{rot} = rotational component of air velocity
V_∞ = freestream air velocity
We_L = Weber number based on model size and water properties (Eq. (15))
β = collection efficiency
β_0 = collection efficiency at stagnation (Eq. (8))
δ = drop median volumetric diameter (MVD)
ϕ = Droplet energy transfer parameter (Eq. (11))
λ = Droplet range
λ_{Stokes} = Droplet range if Stokes Law applies
Λ_f = Latent heat of freezing
Λ_v = Latent heat of condensation
μ = Air viscosity
θ = Air energy transfer parameter (Eq. (12))
ρ = Air density
ρ_i = Ice density
ρ_w = Liquid water density
σ = Surface tension of water over air
τ = accretion time
ω = propeller rotational speed, rad/s

Subscripts

L = undefined length proportional to the model chord
R = reference conditions
S = scale conditions

II. Introduction

A rapidly growing aviation industry called Advanced Air Mobility (AAM) is seeking to provide safe, sustainable, and more accessible air transportation services for both people and cargo to augment current ground modes of transportation. Urban Air Mobility (UAM) is a subset of AAM which is focused on localized missions of up to approximately 120 km (75 miles) within and around metropolitan areas [1]. Many electric vertical takeoff and landing (eVTOL) vehicles have been proposed for UAM due to their energy efficiency and ability to take off and land vertically without the need of conventional airports or runways.

However, for the AAM industry to be successful, it must maintain a high level of operation safety in inclement weather. Icing is one weather hazard related challenge that presents a significant risk to the safe operation of eVTOL vehicles and the scalability of their operations. Currently no icing simulation tools, both experimental and computational, have been validated or developed specifically for eVTOL configurations. Likewise, similar in look to

a propeller the novel open fan engine architecture is the current focus by the Propulsion Technologies sub-project of the NASA Advanced Air Transport Technology project (AATT) and it also needs icing simulation tools.

The results presented here are part of an effort to develop appropriate scaling methods for AAM propeller and open fan engine ice accretion. These scaling methods are needed to determine alternate scale test conditions from the desired (i.e. reference) model sizes or test conditions when they cannot be achieved in a test facility like IRT. Previously, Anderson [2] has given a detailed technical review of recommended scaling methods for ice accretion on unprotected, unswept fixed wing surfaces in Appendix C condition. Later, Anderson and Tsao [3] have further supplemented the methods utilizing additional data from both SLD and Appendix C tests. In a more recent study, Tsao and Lee [4] have further extended the recommended scaling methods for modern swept wing icing applications.

It was concluded from those three references that acceptable ice shape scaling results could be achieved by matching the β_0, A_c, n_0 and We_L for fixed wing configurations. With scale model size selected, by matching scale and reference values of We_L the scale velocity can be determined. By matching β_0 the scale *MVD* can be found. Reference [2] also showed that the effects of temperature and *LWC* are not independent but interact through the freezing fraction. Therefore, with scale *LWC* chosen, by matching n_0 the scale temperature can be calculated. Finally, by matching A_c the scale icing spray cloud time can be established. For the scale test, then, only temperature, velocity, *MVD* and time must be calculated from the known (reference) values of the similarity parameters.

For evaluating propeller icing scaling methods, two IRT test campaigns were completed recently. The March 2023 test, the AAM Rotor Icing Evaluation Study (ARIES) I, was reported by von Hardenberg, *et. al.* [5]. The ARIES II test, a follow-on campaign, was conducted in January 2024. The observations from those tests on ice formations on propeller blades have suggested that although there are distinct morphological feature differences in ensuing ice shapes with feathers on fixed wing and rotating blade surfaces, the fundamental physics of ice accretion appears to be similar. Thus, it is hypothesized that similarity parameters used for fixed wing icing are applicable to propeller icing applications. An additional important similarity parameter for propellers is the advance ratio, *J*, which describes the relationship between the forward air velocity of the propeller and its rotational speed. Matching this parameter is required for flow-field similarity of geometrically similar propellers at the same pitch and the same flow angle of attack setting at the selected reference radial location of r/R. By matching *J*, the scale propeller rotational speed can be determined.

In this paper, a limited number of reference and scale ice shape comparisons obtained from those NACA 0012 airfoil blades at r/R = 0.75 radial location during the ARIES I & II tests were utilized to evaluate how well the proposed scaling methods work in propeller icing situations.

III. Similarity Parameters

The similarity parameters used in this study were based on the work originally done by Ruff [6]. The scaling method involved matching scale and reference values of the key similarity parameters, *J*, β_0, A_c, n_0, and We_L. The equations for the similarity parameters will be presented here without discussion.

To maintain the rotational flow-field similarity of geometrically similar rotating propellers in forward motion, the advance ratio *J* is introduced:

$$J = \frac{V_\infty}{ND} = \frac{2\pi V_\infty}{\omega D} \tag{1}$$

where N is the rotational rate of the propeller in rev/s, ω is the rotational speed of the propeller in rad/s which is equal to 2π N, and D is the diameter of the propeller. Matching this parameter *J* is required for flow-field similarity of geometrically similar propellers at the same pitch and flow angle of attack setting.

One approach, which was first used in [5], is to divide the blade into a discrete number of radially distributed sections to which the recommended icing scaling methods developed for fixed wings can be applied. To calculate the key icing similarity parameters at a given radial location, one must first determine the effective velocity, V_{eff}, that the propeller experiences at that radial location. Due to the rotation and forward velocity of the propeller, the blade experiences both an axial and rotational component of velocity (V_{ax} and V_{rot}, respectively) which varies radially along the blade. The V_{eff} that the blade experiences at a given radial location can be determined by calculating the resultant magnitude of the V_{ax} and V_{rot} components of velocity at that location as seen in Eq. (2).

$$V_{eff} = \sqrt{(V_{ax})^2 + (V_{rot})^2} \tag{2}$$

For this study, it was assumed that the effects of propeller induction could be ignored such that $V_{ax} \approx V_\infty$ and $V_{rot} \approx \omega r$, where V_∞ is the freestream air velocity, and r is the distance from the center of rotation to the radial location of interest. With these assumptions, an approximation for V_{eff} can be obtained using Eq. (3).

$$V_{eff} \approx \sqrt{(V_\infty)^2 + (\omega r)^2} \tag{3}$$

Once a value for V_{eff} is determined at a given radial location, the key icing similarity parameters can be estimated by substituting V_{eff} for V_∞ (or V) during the introductions of those parameters shown below.

To maintain the droplet trajectory similitude, Langmuir and Blodgett [7] introduced the modified inertia parameter, K_0, defined as

$$K_0 = \frac{1}{8} + \frac{\lambda}{\lambda_{Stokes}}\left(K - \frac{1}{8}\right) \tag{4}$$

for $K > 0.125$, to describe the inertia of droplets in an air stream flowing around a cylinder of radius d positioned normal to the flow. In Eq. (4), K is the inertia parameter,

$$K = \frac{\rho_w \delta^2 V_\infty}{18 d \mu} \tag{5}$$

Departing slightly from Langmuir and Blodgett in this study, d represents twice the leading-edge radius of curvature for airfoils. For the NACA 0012 airfoil model, a leading-edge radius of $0.0158c$ was used (see Abbott and von Doenhoff [8]), where c is the airfoil chord. In Eq.(4), λ/λ_{Stokes} is the droplet range parameter, defined as the ratio of actual droplet range to that if Stokes drag law for solid spheres applied. It is a function only of the droplet Reynolds number, Re_δ.

$$Re_\delta = \frac{V \delta \rho}{\mu} \tag{6}$$

This study uses a curve fit to Langmuir and Blodgett's tabulation of the range parameter as given in the following expression:

$$\frac{\lambda}{\lambda_{Stokes}} = \frac{1}{\left(0.8388 + 0.001483 Re_\delta + 0.1874\sqrt{Re_\delta}\right)} \tag{7}$$

Of more practical interest than K_0 is the collection efficiency at the stagnation point, β_0, which was shown by Langmuir and Blodgett to be a function only of K_0,

$$\beta_0 = \frac{1.40\left(K_0 - \frac{1}{8}\right)^{.84}}{1 + 1.40\left(K_0 - \frac{1}{8}\right)^{.84}} \tag{8}$$

Thus, the droplet trajectory similarity is satisfied if $K_{0,S} = K_{0,R}$ and so is $(\beta_0)_S = (\beta_0)_R$, and the scale drop size, i.e. scale *MVD*, is determined.

To ensure water-catch similarity, the accumulation parameter is introduced:

$$A_c = \frac{LWCV\tau}{d\rho_i} \tag{9}$$

If all the water impinging on the leading edge freezes at that location and the leading-edge collection efficiency is 100%, A_c directly becomes a measure of the normalized thickness of ice that will accrete. The scale accretion time can be found from $A_{c,S} = A_{c,R}$. When super-cooled water drops strike an aircraft surface, they may not freeze immediately on impact. The freezing fraction is the ratio of the amount of water that freezes in a specified region on the surface to the total amount of liquid water that reaches that region. Thus, local ice thickness depends on $\beta_{0,\mathcal{N}} A_c$ and freezing

fraction. Because each local ice thickness around the model defines the overall shape of the ice, the freezing fraction obviously has a major influence on ice shape. The freezing fraction is influenced mainly by the ambient temperature, the *LWC* of the cloud and the effective velocity.

The rate at which the water freezes on the surface depends on the magnitude of local heat transfer imbalance. For glaze ice, it is known that the fraction of water mass which freezes is less than unity, and the motion of unfrozen surface water can influence the resulting ice shape. Therefore, it is important to maintain surface energy and surface-water dynamics similarities for glaze ice accretions. The freezing fraction is formally defined as the ratio of the amount of water that freezes at a given surface location to the total amount of water that impinges at that location. From Messinger's [9] steady-state surface energy balance analysis, the freezing fraction at the stagnation point can be written as

$$n_0 = \frac{c_{p,ws}}{\Lambda_f}\left(\phi + \frac{\theta}{b}\right) \tag{10}$$

The key terms in this formulation include ϕ and θ, which have dimensions of temperature and relate to the water drop energy transfer and air energy transfer, and b, the relative heat factor, which was first introduced by Tribus, *et. al*. [10]

$$\varphi = t_f - t_{st} - \frac{V^2}{2c_{p,ws}} \tag{11}$$

$$\theta = \left(t_s - t_{st} - r\frac{V^2}{2c_p}\right) + \frac{h_G}{h_c}\left(\frac{\frac{p_{ww}}{T_{st}} - \frac{p_{tot}}{T_{tot}}\frac{p_w}{p_{st}}}{\frac{1}{.622}\frac{p_{tot}}{T_{tot}} - \frac{p_{ww}}{T_{st}}}\right)\Lambda_v \tag{12}$$

$$b = \frac{LWC\, V\, \beta_0\, c_{p,ws}}{h_c} \tag{13}$$

Equation (12) from Ruff [6] has included compressibility effects. Various incompressible forms of θ have also been used by Charpin and Fasso [11] and others; however, the differences are not significant mainly because, for most icing conditions, the Mach number is relatively low.

In 1988 Bilanin [12] presented a Buckingham-π analysis in which he concluded that surface-water phenomena had to be included in icing scaling methods. Olsen and Walker [13] and Hansman, *et. al.* [14,15,16] studied surface effects and surface water during ice accretion, presenting additional evidence that these were important phenomena to consider in ice accretion. From the close-up photographs of these research studies, it was observed that for glaze ice accretion unfrozen water on the ice surface tended to coalesce to form beads. These beads sometimes were swept downstream and sometimes froze in place. Bilanin [12, 17] also argued that drop splashing on impact might affect the shape of the ice accreted.

Hansman and Turnock [14] found that when a surfactant was added to the icing spray water, the ice shape appearance and shape changed significantly, with the glaze horns moving toward the leading edge. Clearly, then, surface tension, and by implication, surface phenomena, have a significant role in the physics of ice accretion.

In 2003 Anderson and Tsao [18] had provided experimental evidence from past studies to show that a similarity parameter dependent on the ratio $V^x c^y/\sigma^z$ must be included in scaling methodology to account for surface-water dynamics effect in glaze ice accretions, although the powers *x, y* and *z* are not yet determined. The length may not be chord itself but rather some physical characteristic *L* related to chord; for example, the water-film thickness. Thus, a Weber number based on *L* and *V*

$$We_L = \frac{V^2 L \rho_w}{\sigma} \tag{14}$$

has been suggested as a potential additional similarity parameter to supplement Ruff's basic scaling method. Studies by Bartlett [19, 20] and Oleskiw, *et. al*. [21] found no measurable effect of pressure on ice shape. These observations suggest that water density is a better choice than air density for Eq. (14). In this study the We_L is based on twice the nose radius of the airfoil (i.e. $L = d$)

$$We_L = \frac{V^2 d \rho_w}{\sigma} \tag{15}$$

with the understanding that $L \propto d$. The scale velocity found from matching $We_{L,S}$=$We_{L,R}$ is

$$V_S = V_R \left(\frac{d_R}{d_S} \right)^{1/2} \tag{16}$$

IV. Test Article and Instrumentation

A. Propeller Test Stand

A picture of the propeller test stand installed in the IRT test section with the 36 inches diameter blades is shown in Fig. 1 [5].

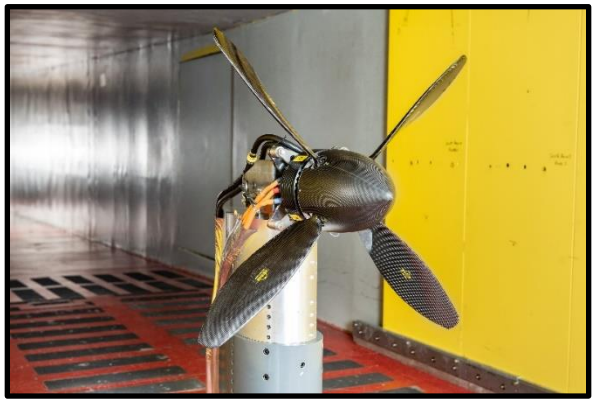

Fig. 1 NASA's eVTOL Propeller Test Stand for Fundamental Icing Physics Studies

The angle between the propeller axis of rotation and the freestream air velocity, known as the propeller incidence angle, can be articulated from 0° (axial flow) to 95° in increments of 5° by adjusting the pitch head on the test stand. The pitch head can also be traversed vertically from 24" - 36" from the test section floor as shown in Fig. 2.

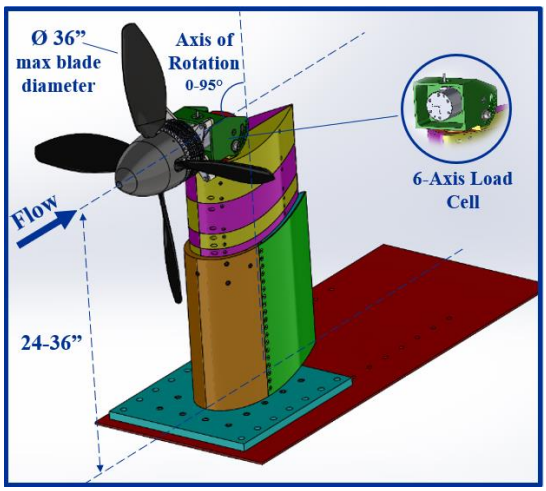

Fig. 2 CAD Model of the Propeller Test Stand Showing Location of Load Cell

This allows the center of rotation of the propeller to remain near the centerline of the test section where the cloud is the most uniform regardless of the pitch head angle setting. The strut, which provides the main structural support of the test stand, is enclosed by a NACA 0040 airfoil for improved airflow characteristics. For the ARIES I & II tests,

the propeller remained in an axial-flow configuration to simulate an eVTOL propeller in a forward flight. The center of rotation of the propeller was located 36” from the floor at the centerline of the test section.

B. Propeller Geometry

Three carbon fiber propellers of diameters 24, 28, and 36 inches were custom-made for the 2023 and 2024 test entries. Those three propellers all had a NACA 0012 airfoil profile and were geometrically scaled from a radial location of roughly r/R = 0.40 to r/R = 1.0. A non-proprietary propeller geometry inspired by the Computationally Optimized Proprotor (COPR) design and developed by NASA was used [22]. It should be noted, though, that the nominal COPR twist and chord distributions were adjusted for manufacturing feasibility purposes, and so the final design of the propeller blades used for this experiment are not perfect representations of the original COPR design. The final twist and chord distributions of the three propellers used during this experiment are shown in Fig. 3 [5].

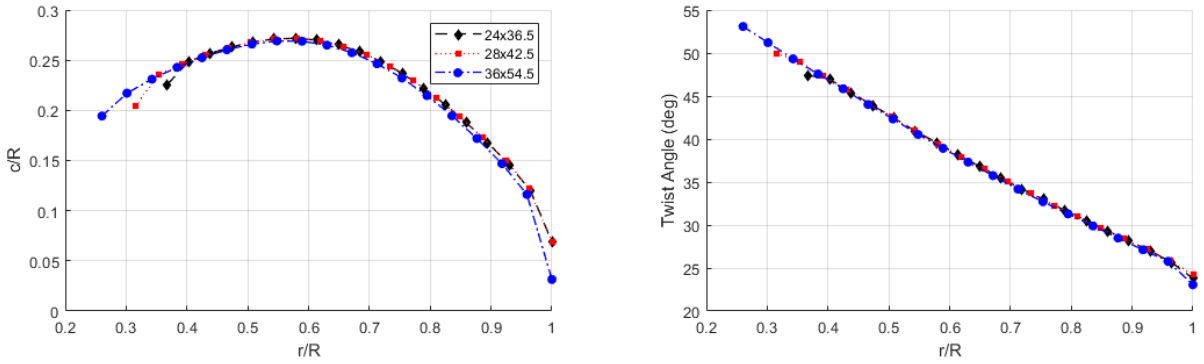

(a) Chord Distributions **(b) Twist Angle Distributions**

Fig. 3 Comparisons of the propeller chord (a) and twist angle (b) distributions between the three propeller sizes.

It can be seen from Fig. 3 that the three propellers have similar normalized twist and chord distributions from a radial location of approximately r/R = 0.40 to r/R = 1.0. The use of the same hub and spinner for each set of propeller blades prevented geometric similarity towards the root of the blade. In a companion CFD study by Rigby and von Hardenberg [23], the effect of keeping the centerbody spinner size constant while varying the propeller size was found to have a small effect on the pressure distribution but have a negligible effect on the predicted rime ice shapes from GlennICE simulations. In addition, Fig. 4 provides some physical insight on how n_0^* (the theoretical freezing potential) varied radially along the span of the blade in a freestream total air temperature sweep [5]. For a propeller with a constant chord distribution, n_0^* is expected to be the lowest at the tip of the blade where the propeller experiences the highest V_{eff}. However, due to the tapering chord of the propeller used in this study, n_0^* was found to increase towards the tip of the blade. As a result, the lowest value of n_0^* tended to occur between r/R = 0.70 and r/R = 0.80.

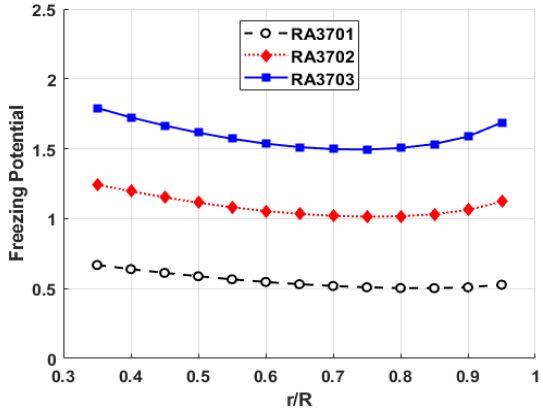

Fig. 4 Theoretical Freezing Potential vs r/R Distribution for Runs RA3701, RA3702, and RA3703 [5].

Additionally, it was noticed during the ARIES I test campaign [5] that the calculated freezing fraction values seemed to be over-estimated in terms of the typical ice shape associated with a known freezing fraction value. Further examination from the cold clean scans of those three propeller blades (i.e. 24", 28" and 36" blades) in the post-test data analysis revealed that the design NACA 0012 airfoil leading edge profile of d/c=0.0317 were not met. Instead, they were all greater than this set value by 70%, 32% and 20% respectively which in part helped to explain why the calculated freezing fraction seemed to be over-estimated in terms of the typical ice shape associated with a known freezing fraction value. Thus, for the future test campaigns, better control of manufacturing new NACA 0012 propeller blade models will be required to ensure the design leading edge profile will be met with acceptable tolerance.

Another potential physical factor to reduce the freezing fraction value is the convective heat transfer coefficient correlation used is this study, which may need to be modified for the much lower model Reynolds number regime (~ 2 $x10^4$) experienced by those smaller NACA 0012 airfoil propeller blades. This factor is beyond the scope of this study and requires further investigation.

V. Test Description

A. Icing Research Tunnel

The tests were performed in the NASA Glenn Icing Research Tunnel [24]. The IRT is a closed-loop, refrigerated, sea level tunnel with a test section size of 1.8 x 2.7 m (6 x 9 ft). A tunnel schematic is shown on Fig. 5. The icing cloud is generated by operating 10 spray bars upstream of the test section. The calibrated speed range of the IRT is from 50 to 300 knots (in empty test section) [25]. Ballistic panels were installed on the walls of the tunnel test section to protect personnel in the control room during operation of the propeller. A Phantom v2640 high-speed camera was installed above the test section and upstream of the propeller test stand to capture ice shedding events.

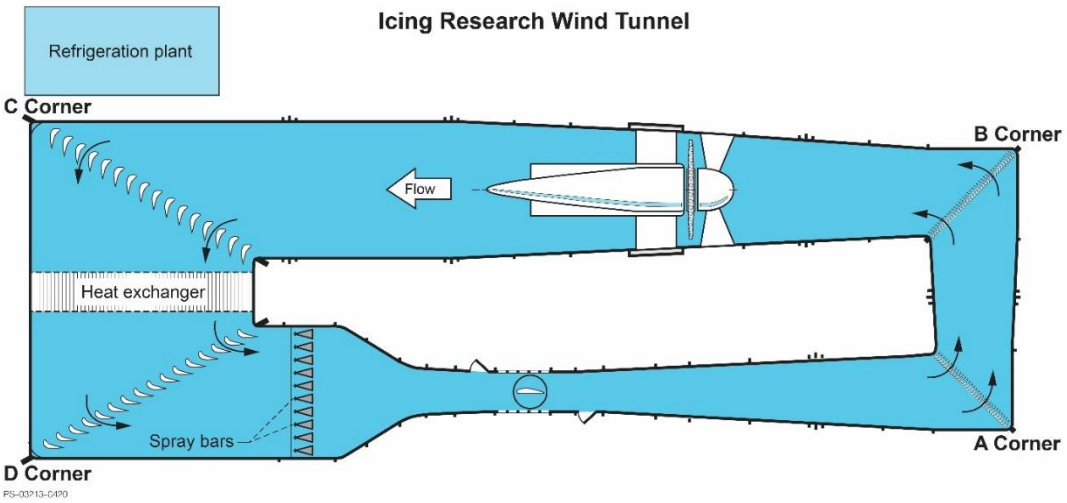

Fig. 5 Schematic of the Icing Research Tunnel.

B. Icing Test Procedure

A typical run consisted of increasing the propeller RPM incrementally followed by tunnel speed up to the target conditions for that run. The increments at which the propeller RPM and tunnel speed increased were chosen such that the propeller avoided a windmilling condition which could potentially damage electronic hardware due to the reverse flow of electrical power (a brake resistor was later installed near the end of test entry which could dissipate the power generated during a windmilling scenario). The incremental approach also allowed for system health checkouts to be performed before moving to a higher speed condition.

Once the target propeller RPM and tunnel speed were reached, the tunnel operators would wait until the tunnel has reached the target tunnel temperature before initiating the spray. During the spray, model vibrational loads were monitored to ensure that the safe operating limits were not exceeded. Once the planned spray time was achieved for that run, the spray was turned off and a similar incremental approach was conducted to reduce the propeller and tunnel speed, this time starting with a decrease in tunnel speed followed by propeller RPM. Once the propellers were completely stopped, researchers entered the test section to document the ice shape.

The documentation process included taking various still images of the iced model, scanning of ice shapes, and collecting ice mass measurements. It was assumed that there would be little blade to blade difference in noticeable ice shape features, and thus only one blade was scanned for each run. Each blade was numbered to ensure that the same blade was scanned every time. Afterwards, the ice from the scanned blade was scraped into a bucket and weighed. The spinner, which could be quickly removed from the model via four screws, was weighed after each run to document the spinner ice mass. Finally, any remaining ice was removed from the model using isopropyl alcohol and prepped for the next run.

VI. Test Results

A. Test Conditions

Due to limited IRT test time available for the scaling method evaluation only three sets of scaling test data were obtained: (1) a simplified model size scaling evaluation test was performed in a rime ice condition on those three geometrically similar propellers of different diameters and (2) a *LWC* condition scaling test was evaluated in a nominal glaze ice condition for the 28" diameter propeller during the March 2023 ARIES I test entry in the IRT. In the January 2024 IRT test entry, (3) another *LWC* condition scaling evaluation run was performed on the 36" diameter propeller.

For these tests, the median volumetric diameter (*MVD*) ranged from 15 to 80 μm, the liquid water content (*LWC*) ranged from 0.55 to 1.20 g/m3, the tunnel speed ranged from 80 to 130 knots, and the total air temperature ranged from -3 to -18°C which provided the stagnation point freezing fraction (n_0) of 0.51 to 1.0. The propeller helical tip speeds for these tests ranged from 68.5 to 107.6 m/s, and the advance ratios ranged from 2.32 to 2.79. The ice shape scaling evaluation results on those AAM propellers are presented with 2D ice shapes extracted from 3D laser scans of those iced propellers at the selected reference radial location of r/R = 0.75. Repeat runs were performed for some icing conditions with the purpose of acquiring sufficient ice shapes to test repeatability.

B. Model Size Scaling

It is recommended to evaluate the scaling methods in rime conditions which will produce a well-known rime ice shape as part of the overall assessment on how effective the scaling methods are in the IRT. For the rime ice simulations on those three geometrically similar propellers the reference (i.e. RA3717) and scale (i.e. RA3698 & RA3681) test conditions were determined in the following simplified manner : the drop *MVD, LWC* and air velocity V_∞ were held constant for all three propellers, and the air temperature were held constant at a sufficiently cold value such that the stagnation point freezing fraction n_0 was 1.0 at the r/R=0.75 reference location but also across the entire propeller span. The reference and scale test spray times were calculated by holding the ($\beta_0 A_c$) product constant, and the reference and scale propeller RPMs were determined by matching advance ratio and each propeller was set to the same target pitch setting. As seen from Fig. 6, reasonably good agreement between the rime ice shapes was achieved.

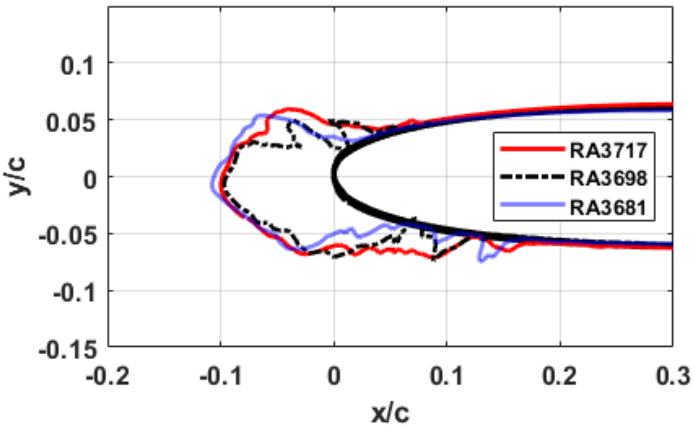

Fig. 6 Model Size Scaled Ice Shape Comparison at r/R = 0.75

Table 1 Planned Model Size Scaling Test Conditions in ARIES I

	Target Operating and Cloud Conditions								Similarity Parameters (calculated at r/R = 0.75)			
Run	V_∞ knots	$t_{\infty,0}$ °C	δ μm	LWC g/m^3	τ min	RPM rev/min	D in	J	n_0	A_c	β_0	We_L 10^6
RA3717	95	-12.0	15	0.55	3.4	1928	24	2.49	1.0	3.76	0.90	0.15
RA3698	"	"	"	"	4.0	1657	28	2.49	1.0	3.78	0.89	0.18
RA3681	"	"	"	"	5.0	1300	36	2.47	1.0	3.67	0.86	0.23

It should be noted that more data is needed to assess the effectiveness of the size scaling method, especially at n_0 < 1.0 where the glaze ice accretion is much more sensitive to the interaction between the accretion process and the surface unfrozen runback water dynamics set by n_0 and We_L.

C. *LWC* Condition Scaling

LWC is an important icing parameter as it not only affects the rate of ice accretion, but also the ice shape that forms due to its strong effect on the freezing fraction. Figure 7 illustrates the appropriate condition scaling consideration of increasing the *LWC* from 0.55 to 1.2 g/m^3 at a freezing fraction of n_0 = 0.51 for the 28" diameter propeller. As the Olsen method for *LWC* condition scaling required, the icing spray time was adjusted to match A_c between the reference and scale *LWC* runs. The air temperature was adjusted to maintain the same freezing fraction n_0 = 0.51. As seen from Fig. 7, good agreement between the ice shapes was achieved.

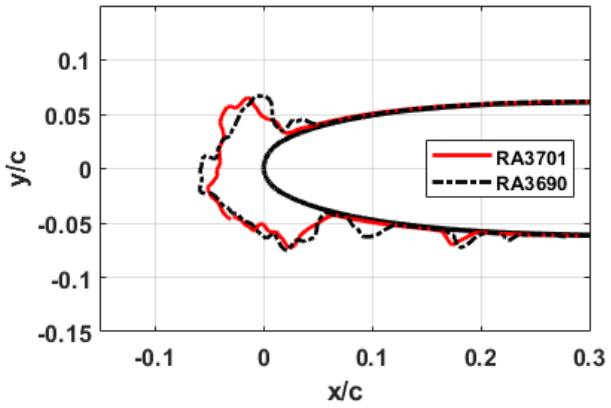

Fig. 7 *LWC* Scaled Ice Shape Comparison at r/R = 0.75 in ARIES I

Table 2 Planned *LWC* Scaling Test Conditions in ARIES I

	Target Operating and Cloud Conditions								Similarity Parameters (calculated at r/R = 0.75)			
Run	V_∞ knots	$t_{\infty,0}$ °C	δ μm	LWC g/m^3	τ min	RPM rev/min	D in	J	n_0	A_c	β_0	We_L 10^6
RA3701	87	-3.0	15	0.55	3.0	1516	28	2.49	0.51	2.59	0.88	0.15
RA3690	"	-6.0	"	1.20	1.4	"	"	"	"	2.64	"	"

Figure 8 shows another *LWC* condition scaling test results of varying the *LWC* from 0.65 to 0.8 and then to 1.2 g/m^3 at a freezing fraction of n_0 = 0.94 for the 36" diameter propeller. As the Olsen method for *LWC* condition scaling

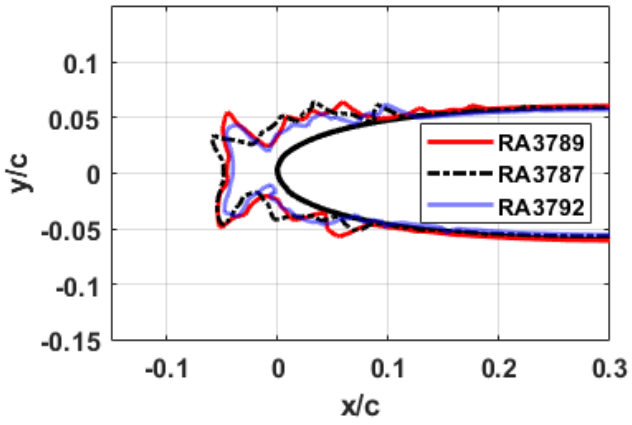

Fig. 8 *LWC* Scaled Ice Shape Comparisons at r/R = 0.75 in ARIES II

Table 3 Planned *LWC* Scaling Test Conditions in ARIES II

	Target Operating and Cloud Conditions								Similarity Parameters (calculated at $r/R = 0.75$)			
Run	V_∞ knots	$t_{\infty,0}$ °C	δ μm	*LWC* g/m^3	τ min	*RPM* rev/min	*D* in	*J*	n_0	A_c	β_0	We_L 10^6
RA3789	110	-8.2	20	0.65	2.1	1330	36	2.79	0.94	1.99	0.91	0.28
RA3787	"	-10.0	"	0.80	1.7	"	"	"	"	"	"	"
RA3792	"	-13.3	"	1.1	1.2	"	"	"	0.93	1.93	"	"

required, the icing spray time was adjusted to match A_c between the reference and scale *LWC* runs. The air temperature was adjusted to maintain the same freezing fraction n_0 = 0.94. As seen from Fig. 8, good agreement between the ice shapes were achieved. It should be noted that the planned freezing fraction values shown in Table 2 & 3 were based on the design NACA 0012 airfoil leading edge profile of d/c=0.0317 but measurements of the actual 28" and 36" diameter propellers showed larger values of d/c. As a result, the actual freezing fraction values are smaller which would qualitatively match the typical ice shape associated with a known freezing fraction value. The good agreement between the reference and scale ice shapes from the *LWC* condition scaling tests would suggest that the existing scaling methods developed for fixed-wings should be applicable to rotating propeller blades.

While the results of the recommended scaling methods obtained from ARIES I and II test entries are encouraging, more data is needed to assess the effectiveness of the scaling methods, especially at freezing fractions less than unity where the ice shape is more sensitive to temperature and surface runback water dynamics. In addition, demonstration of the scaling methods over a larger range of propeller sizes and operating conditions is needed to provide greater confidence in the scaling method applications.

VII. Conclusion

Limited icing tests were performed in the Icing Research Tunnel at NASA Glenn Research Center to evaluate the current proposed scaling methods for propeller icing scaling. The preliminary results showed the scaling methods are effective. Further evaluation of the scaling methods over a wider flow/icing cloud conditions as well as different propeller sizes operating at various advance ratios is recommended to assess its applicability for modern propeller and novel engine fan (i.e. open rotor fan) icing scaling analysis.

The scaling methods developed for unprotected fixed-wing surfaces were explored for use on the propeller with promising results over the range of test conditions including the median volumetric diameter (*MVD*) ranged from 15 to 80 μm, the liquid water content (*LWC*) ranged from 0.55 to 1.20 g/m3, the tunnel speed ranged from 80 to 130

knots, and the total air temperature ranged from -3 to -18°C which provided the stagnation point freezing fraction (n_0) of 0.51 to 1.0. The propeller helical tip speeds for these tests ranged from 68.5 to 107.6 m/s, and the advance ratios ranged from 2.32 to 2.79. The key icing similarity parameters calculated at r/R = 0.75 for each run are provided in the paper. The calculated freezing fraction appeared to overestimate the true value of freezing fraction because the actual models were not of the NACA 0012 airfoil profile as design. More work is needed to assess the effectiveness of the scaling approach, especially for freezing fractions less than unity. In addition, demonstration of the scaling methodology over a larger range of propeller sizes and operating conditions is needed to provide greater confidence in the scaling methodology and its application to the modern propeller and engine open rotor fan.

Acknowledgments

The authors wish to acknowledge the financial support for this work by the Propulsion Technologies sub-project of the NASA Advanced Air Transport Technology project (AATT) under NASA's Advanced Air Vehicles Program (AAVP). The authors would also like to acknowledge all of those who helped make this a successful test. In particular, the authors would like to thank Keith Hunker, Xavier Collazo Fernandez, Joe Wisniewski, and Scott Hensley for their invaluable technical support. The authors would also like to thank Jordan Salkin and Quentin Schwinn for their imaging support during testing. In addition, this work could not have been possible without the support of the NASA Glenn Icing Branch and the IRT engineers and technicians for their efforts in making these test campaigns a success.

References

[1] Garrow, L. A., German, B., Schwab, N. T., Patterson, M. D., Mendonca, N., Gawdiak, Y. O. and Murphy, J. R., "A Proposed Taxonomy for Advanced Air Mobility," *AIAA AVIATION 2022 Forum*, AIAA Paper 2022-3321, Chicago, IL, June-July 2022.

[2] Anderson, D. N., "Manual of Scaling Methods," NASA /CR–2004-212875, March 2004.

[3] Anderson, D. N and Tsao, J. C., "Ice Shape Scaling for Aircraft in SLD Conditions," NASA/CR-2008-215302 and DOT/FAA/AR-07/55, September 2008.

[4] Tsao, J. C. and Lee, S., "Evaluation of Icing Scaling on Swept NACA 0012 Airfoil Models," NASA/CR-2012-217419, May 2012.

[5] von Hardenberg, P.H., Flack, C.A., and Rigby, D.L., "Ice Shape Analysis of an eVTOL Propeller in Forward Flight at the NASA Glenn Icing Research Tunnel," AIAA AVIATION 2024 Forum, AIAA Paper 2024-4448, Las Vegas, NV, July-August 2024.

[6] Ruff, G.A., "Analysis and Verification of the Icing Scaling Equations," AEDC-TR-85-30, vol 1 (rev), March 1986.

[7] Langmuir, Irving and Blodgett, Katharine B. "A Mathematical Investigation of Water Droplet Trajectories," Army Air Forces Technical Report No. 5418, February 1946.

[8] Abbott, Ira H. and von Doenhoff, Albert E., Theory of Wing Sections, Dover, New York, 1959, pp114 and 321.

[9] Messinger, B.L., "Equilibrium Temperature of an Unheated Icing Surface as a Function of Airspeed," J. Aeron. Sci., vol. 20 no. 1, January 1953, pp 29 – 42.

[10] Tribus, Myron, Young, G.B.W. and Boelter, L.M.K., "Analysis of Heat Transfer Over a Small Cylinder in Icing Conditions on Mount Washington," Trans. ASME, vol. 70, November 1948, pp 971 – 976.

[11] Charpin, Francois and Fasso, Guy, "Essais de givrage dans la grande soufflerie de Modane sur maquettes a echelle grandeur et echelle reduite," L'Aeronautique et l'Astronautique, no. 38, 1972, pp 23 – 31. English translation published as "Icing Testing in the Large Modane Wind-Tunnel on Full-Scale and Reduced Scale Models," NASA TM-75373, March 1979.

[12] Bilanin, A. J., "Proposed Modifications to the Ice Accretion/Icing Scaling Theory," AIAA-88-0203, January 1988.

[13] Olsen, W. and Walker, E., "Experimental Evidence for Modifying the Current Physical Model for Ice Accretion on Aircraft Surfac-es," NASA TM 87184, 1986.

[14] Hansman, R. John, Jr. and Turnock, Stephen, R., "Investigation of Surface Water Behavior During Glaze Ice Accretion," J. Air-craft, vol. 26 no. 2, February 1989, pp 140-147.

[15] Hansman, R. John, Jr. and Turnock, Stephen R., "Investigation of Microphysical Factors which Influence Surface Roughness Dur-ing Glaze Ice Accretion," 4th International Workshop on Atmospheric Icing of Structures, Paris, September 1988.

[16] Hansman, R.J., Breuer, K.S., Hazan, D., Reehorst, A. and Vargas, M., "Close-up Analysis of Aircraft Ice Accretion," AIAA-93-0029, January 1993.

[17] Bilanin, Alan J. and Anderson, David N., "Ice Accretion with Varying Surface Tension," AIAA-95-0538 and NASA TM 106826, January 1995.

[18] Anderson, David N. and Tsao, J.C., "Additional Results of Ice-Accretion Scaling at SLD Conditions," AIAA-2003-0390, January 2003.

[19] Bartlett, C. Scott, "An Analytical Study of Icing Similitude for Aircraft Engine Testing," DOT/FAA/CT-86/35 and AEDC-TR-86-26, October 1986.

[20] Bartlett, C. Scott, "Icing Scaling Considerations for Aircraft Engine Testing," AIAA-88-0202, January 1988.

[21] Oleskiw, Myron M., De Gregorio, Fabrizio and Esposito, Biagio, "The Effect of Altitude on Icing Tunnel Airfoil Icing Simulation," Proceedings of the FAA International Conference on Aircraft Inflight Icing, DOT/FAA/AR-96/81,II, August 1996, pp 511 – 520.

[22] Zawodny, N. S., Pettingill, N. A., Lopes, L. V., and Ingraham, D, J., "Experimental Validation of an Acoustically and Aerodynamically Optimized UAM Proprotor Part 1: Test Setup and Results," NASA/TM-20220015637, 2023.
[23] Rigby, D. L. and von Hardenberg, P. H., "GlennICE Simulation of 24, 28, and 36 Inch Diameter eVTOL Propellers in Forward Flight," AIAA AVIATION 2024 Forum, Las Vegas, NV, July-August 2024.
[24] Soeder, R. H., Sheldon, D. W., Ide, R. F., Spera, D. A., and Andracchio, C. R., "NASA Glenn Icing Research Tunnel User Manual," NASA/TM-2003-212004, 2003.
[25] Timko, E. N., King-Steen, L. E., Van Zante, J. F., and Acosta, W. J., "NASA Glenn Icing Research Tunnel: 2019 Cloud Calibration Procedure and Results," NASA/TM-20205009045, 2021.